EFDA–JET–PR(08)53

Y. Liang, H.R. Koslowski, P.R. Thomas, E. Nardon, S. Jachmich, A. Alfier, G. Arnoux, Y. Baranov, M. Bcoulet, M. Beurskens, R. Coelho, Th. Eich, E. De La Luna W. Fundamenski, S. Gerasimov, C. Giroud, M.P. Gryaznevich, D. Harting, A. Huber, A. Kreter, L. Moreira, V. Parail, S.D. Pinches, S. Saarelma, O. Schmitz and JET EFDA contributors

Active Control of Type-I Edge Localized Modes with $n = 1$ and $n = 2$ Fields on JET

Active Control of Type-I Edge Localized Modes with $n = 1$ and $n = 2$ Fields on JET

Y. Liang[1], H.R. Koslowski[1], P.R. Thomas[2], E. Nardon[3], S. Jachmich[4], A. Alfier[5], G. Arnoux[6], Y. Baranov[3], M. Bcoulet[6], M. Beurskens[3], R. Coelho[7], Th. Eich[8], E. De La Luna[9], W. Fundamenski[3], S. Gerasimov[3], C. Giroud[3], M.P. Gryaznevich[3], D. Harting[1], A. Huber[1], A. Kreter[1], L. Moreira[3], V. Parail[3], S.D. Pinches[3], S. Saarelma[3], O. Schmitz[1] and JET EFDA contributors*

JET-EFDA, Culham Science Centre, OX14 3DB, Abingdon, UK

[1] Forschungszentrum Jülich GmbH, Association EURATOM-FZ Jülich, Institut für Energieforschung Plasmaphysik, Trilateral Euregio Cluster, D-52425 Jülich, Germany
[2] Fusion for Energy Joint Undertaking, Josep Pl. 2, Torres Diagonal Litoral B3, 08019, Barcelona, Spain
[3]EURATOM-UKAEA Fusion Association, Culham Science Centre, OX14 3DB, Abingdon, OXON, UK
[4]Association EURATOM-Belgian State, Koninklijke Militaire School - Ecole Royale Militaire, B-1000 Brussels Belgium
[5]Associazione EURATOM-ENEA sulla Fusione, Consorzio RFX Padova, Italy
[6] Association EURATOM-CEA, 13108 St Paul-lez-Durance, France
[7]Associao EURATOM/IST, Centro de Fuso Nuclear, Instituto Superior Tcnico, Av Rovisco Pais, 1049-001 Lisbon, Portugal
[8] Max-Planck-Institut für Plasmaphysik, EURATOM-Assoziation, D-85748 Garching, Germany
[9] Asociacin EURATOM-CIEMAT, Avenida Complutense 22, E-28040 Madrid, Spain
** See annex of F. Romanelli et al, "Overview of JET Results", (Proc. 22 [nd] IAEA Fusion Energy Conference, Geneva, Switzerland (2008)).*

Preprint of Paper to be submitted for publication in
Nuclear Fusion

ABSTRACT.
Recent experiments on JET have shown that type-I Edge Localized Modes (ELMs) can be controlled by applying static low n = 1 external magnetic perturbation fields produced by four external Error Field Correction Coils (EFCC) mounted far away from the plasma between the transformer limbs. When an n = 1 field with an amplitude of a few Gauss at the plasma edge (>0.95) is applied during the stationary phase of a type-I ELMy H-mode plasma, the ELM frequency rises from ~30Hz up to ~120Hz and follows the applied perturbation field strength. The energy loss per ELM normalised to the total stored energy, ΔW_{ELM} /W, decreased from 7% to below the resolution limit of the diamagnetic measurement (~2%). Transport analysis using the TRANSP code shows no or a modest reduction of the thermal energy confinement time because of the density pump-out, but when normalised to the IPB98(y, 2) scaling the confinement shows almost no reduction. Stability analysis of mitigated ELMs shows that the operational point moves from intermediate n peeling-ballooning (wide mode) boundary to low-n peeling (narrow mode) boundary with n = 1 perturbation fields. The first results of ELM control with the n = 2 fields on JET demonstrate that the frequency of ELM can be increased by a factor of 3.5, limited by the available EFCC coil current. During the application of the n = 1, 2 fields, a reduction in the ELM size (ΔW_{ELM}) and ELM peak heat fluxes on the divertor target by roughly the same factor as the increase of the ELM frequency has been observed. The reduction in heat flux is mainly due to the drop of particle flux rather than the change of the electron temperature. Similar plasma braking effect has been observed with n = 1 and n = 2 external fields when a same EFCC coil current was applied. Compensation of the density pump-out effect has been achieved by means of gas fuelling in low triangularity plasmas. An optimised fuelling rate to compensate the density pump-out effect has been identified. Less additional toroidal rotation braking and density pump-out due to an application of magnetic perturbation has been observed in plasmas with large TF ripple of 0.8%. Active ELM control by externally applied fields offers an attractive method for next-generation tokamaks, e.g. ITER.

1. INTRODUCTION

The standard tokamak H-mode, which is foreseen as the ITER baseline operating scenario [1], is characterised by a steep plasma pressure gradient and associated increased current density at the edge transport barrier which exceeds a threshold value to drive MagnetoHydroDynamic (MHD) instabilities referred to as Edge Localized Modes (ELMs) [2, 3]. The so-called Type-I ELMs leads to a periodic expulsion of a considerable fraction of the stored energy content onto the plasma facing components. The periodic and transient expulsion of energy onto plasma facing components is predicted to be too high and will pose a severe problem for the integrity and lifetime of these components. Melting or high erosion rates might occur under certain conditions, as it is derived from extrapolations based on present knowledge [4]. Therefore, reliable methods for the control of Type-I ELM power losses are required for operation of a future fusion machine, e.g. ITER [1].

Previous experiments on DIII-D have shown that the application of Resonant Magnetic

Perturbation fields (RMP) is a promising technique for the complete suppression of ELMs with an $n = 3$ field induced by a set of in-vessel coils [5, 6]. On JET, active control of the transient heat loads due to large type-I ELMs has been achieved with low-n ($n = 1$ and $n = 2$) perturbation fields induced by the set of Error Field Correction Coils (EFCCs) [7, 8, 9] mounted outside of the vacuum vessel [10]. When an $n = 1$ external magnetic perturbation field with an amplitude of a few Gauss at the plasma edge (> 0.95) is applied during the stationary phase of a type-I ELMy H-mode plasma, the ELM frequency rises from ~30Hz up to ~120Hz and follows the applied perturbation field strength [7]. ELM control does not depend on the orientation respect to the vacuum vessel of the applied $n = 1$ magnetic fields. Active control of type-I ELMs with $n = 1$ fields has been developed for more ITER-relevant configurations and parameters in a wide operational space of plasma triangularity (δ up to 0.45), q_{95} (4.8-3.0) and beta (β_N up to 3.0) on JET [8, 11]. The results of ELM control with the $n = 2$ fields on JET demonstrate that the frequency of ELM can be increased by a factor of 3.5, only limited by the available EFCC coil current. A wide operational window of q_{95} has also been obtained for ELM control with either $n = 1$ or $n = 2$ fields [8].

2. EXTERNAL MAGNETIC PERTURBATION FIELD INDUCED BY EFCCS ON JET

On JET, external perturbation fields can be applied by the EFCCs [10]. The system consists of four square shaped coils (~6 m in dimension) which are mounted at equally spaced toroidal positions and attached to the transformer yokes as shown in figure 1. Each coil spans a toroidal angle of 70 degree and has a radial distance along the winding of 5.3 to 7m from the axis of the machine. It has 16 turns and the maximum total coil current amounts to $I_{EFCC} = 48$kAt. Here, the total current is given in terms of the current in one coil winding times the number of turns. Depending on the wiring of the EFCCs either $n = 1$ or $n = 2$ fields can be created. In fact, the EFCCs system on JET was originally designed for compensation in both amplitude and phase of the n = 1 harmonic of the intrinsic error field arising from imperfections in the construction or alignment of the magnetic field coils.

Previous studies of the error field on JET show that the amplitude of the intrinsic error, $B^{err}_{n=1}(q = 2)/B_0$, is only in the order of 10¡5 [12] which corresponds to a few kAt of EFCC current. The effective radial resonance magnetic perturbations, $|b^{res}_{r,eff}| = |B^{res}_{r,eff}/B_0|$, calculated for $I_{EFCC} = 1$kAt in both $n = 1$ and $n = 2$ configurations are shown in figure 1, where $B^{res}_{r,eff}$ and B_0 are the radial resonant magnetic perturbation field and the toroidal magnetic fields, respectively [8]. In the $n = 1$ EFCC con¯guration, the amplitude of the $n = 1$ harmonic is one or two magnitudes larger than other components ($n = 2, 3$). Although the amplitude of $b_{r,eff}$ ($n = 2$) in $n = 2$ EFCCs is by a factor of 3 smaller than $b_{r,eff}$ ($n = 1$) in $n = 1$ EFCCs, the number of resonant surfaces increased by a factor of two and the distances between resonant surfaces are reduced too.

Figure 2 (upper and lower) shows also two examples of combined Poincar and laminar plot for $n = 1$ and $n = 2$ EFCC configuration. These initial results clearly exhibit the stochastic nature of the field line behaviour. The region around the X- point is su±ciently stochastic and the lobes of the

stable and unstable manifolds step out[13]. These field line trajectories caused by the combination of the resonant island chains and the divertor X-point are immanent indication of a resonant destruction of the magnetic field and by that of edge ergodisation. Here, the calculation is based upon an equilibrium reconstruction for Pulse No: 67954 on JET with the perturbing field in vacuum superimposed. Screening effects due to plasma rotation have been neglected.

3. EXPERIMENTAL RESULTS OF ELM CONTROL WITH THE LOW β_N PERTURBATION FIELDS ON JET

3.1. ELM control with n = 1 field in a high triangularity plasma

An overview on an ELM control pulse is shown in ¯gure 3. The traces are (*a*) the total input power, *Ptot* , and the total stored energy, E_{dia}, (*b*) upper and lower plasma triangularity, δ_U, δ_L, (*c*) I_{EFCC}, (*d*) the line-integrated electron densities $n_e l$, measured with an interferometer along two lines of sight, one close to the magnetic axis (upper trace) and the other near the pedestal top (lower trace) (the integration lengths of core and edge probing beams are ~3.2 m and ~1.5 m, respectively), (*e*) electron temperature in the core and near the pedestal top, (*f*) the D_α signal measured at the inner divertor. The pulse had a toroidal magnetic field of B_t = 2.1 T and a plasma current of I_p = 1.8MA, corresponding to an edge safety factor of q_{95} = 4.0. In these experiments, the type-I ELMy H-mode plasma with a high triangularity shape (δ_U = 0.45 and δ_L = 0.4) was sustained by Neutral Beam Injection (NBI) with an input power of 7.5 MW for ~10 s. The electron collisionality at the pedestal is ~0.2. No additional gas fuelling was applied during the H-mode phase. The n = 1 perturbation field created by the EFCCs has a flat top with I_{EFCC} = 32kAt for 2s, which is by a factor of » 8 longer than the energy confinement time of this pulse. Here, the EFCC coil current is only limited due to the I^2t thermal rating limit of the power supplies. During the EFCC phase, the D_α signal (*f*) measuring the ELMs showed a strong reduction in amplitude. The ELM frequency increased from ~30Hz to ~120Hz, while the periodic energy loss due to the ELM crashes normalized to the total stored energy, $\Delta W/W$, measured by the fast diamagnetic loop, indicates a strong reduction from ~8% to values below the noise level (< 2%) of the diagnostic. A continuous decrease in the electron density is observed in the core and edge line-integrated electron density signals even during the °at top of I_{EFCC}. A modest drop (a few per cent) in the total stored energy has been observed during the ELM control phase with the EFCCs.

Figure 4 shows edge profiles of (*a*) T_e, (*b*) n_e and (*c*) electron pressure p_e plotted in the normalized flux coordinate measured by using the High Resolution Thomson Scattering (HRTS) diagnostic from the same discharge shown in Fig.3 [14]. The electron density at pedestal decreases by ~20% due to so called density pump-out [15] during the application of the n = 1 fields, while the pedestal electron temperature increases keep the pedestal pressure almost in constant. However, the pedestal pressure gradient obtained from the derivative of the fit shows that the maximum pressure gradient profile is decreased by 20% during the application of the n = 1 field, and the edge pressure barrier is 20% wider: This is an effect mostly ascribable the strong decrease in *ne* pedestal height with an

almost unvaried width. To identify the character of the mitigated ELMs a heating power scan with four different levels of NBI power, P_{NBI}, of 10, 11.2, 14, 15.2MW has been carried out. The target plasma was operated with ITER baseline scenario ($q_{95} = 3$) with I_p of 2MA and B_t of 1.85T. Figure 5 shows the ELM frequency as a function of P_{NBI}. The frequency of the mitigated ELMs increases when *PNBI* is increased. The power dependence of the ELM frequency is similar to normal type-I ELMs (as shown in the case without $n = 1$ field). However, the mitigated ELMs with $n = 1$ field have a higher frequency and are smaller in size.

The stability analysis using the ELITE code shows that the ELM triggering instability is changed from intermediate-n ($n = 15$) peeling-ballooning mode (driven by both the current density and the pressure gradient) into a low-n ($n = 3$) peeling mode (driven only by the current density) [16]. The most unstable mode width decreases from 3% of the poloidal flux as the plasma crosses the stability boundary while during the edge stochastisation, the mode width grows gradually from almost zero as the stability boundary is crossed, i.e. the modes that become unstable first, thus triggering the ELM, are very narrow (~1% of the poloidal flux) in radial extent. Assuming that the width of the ELM triggering instability (i.e. the width of the most unstable mode) affects the ELM size, this could explain why the ELM size is reduced at the activation of the $n = 1$ field.

3.2. ELM CONTROL WITH $\beta_N = 2$ FIELD ON JET

ELM control with $n = 2$ fields induced by the EFCCs has been carried out on JET [8]. Figure 6 shows the time traces of P_{NBI}, I_{EFCC}, $n_e l$, T_e) and Intensity of D_α signal for a typical ELM control with $n = 2$ fields experiment on JET. The target plasma ($I_p = 1.6$MA; $B_t = 1.85$T; $q_{95} = 4.0$) was heated by NBI with $P_{NBI} = 9$MW. Similar to that observed in the discharges of ELM control with $n = 1$ field, clear pump-out effect and increasing of T_e at plasma core have been observed during application of $n = 2$ fields with $I_{EFCC} = 24$kAt. The frequency of ELMy increased from 15Hz to 40Hz with n = 2 field applied while the temperature drop due to ELM at pedestal was reduced from 650eV to 250eV.

No locked mode has been observed with $n = 2$ fields within the capability of EFCC system on JET. This indicates a wide operation window of ELM control with $n = 2$ fields respecting to that with the $n = 1$ fields where the maximal amplitude of the $n = 1$ fields for ELM control is limited by the locked mode threshold in a low q_{95} plasma.

Figure 7 shows the reduction factor of the peak divertor surface temperature (square) and peak heat flux (diamond) measured by an IR camera viewing the outer strike point as a function of the increases of ELM frequency with an application of the $n = 2$ field [9, 17]. During the application of the $n = 2$ fields, the ELM peak heat fluxes on the divertor target reduces by a roughly the same factor as the increase of the ELM frequency. It is consistent with the reduction in the ELM size (ΔW) by the same factor. The reduction in heat flux is mainly due to the drop of particle flux rather than the change of the electron temperature. Here, the heat fluxes are measured by both Langmuir probes embedded in the divertor tiles and a fast IR camera viewing the divertor targets. A reduction

in the particle flux has been also observed on the outer limiter during the ELM control with perturbation field as shown in Fig.8. The normalized number of larger ELMs indicated with a lager particle flux reduced significantly which benefits the life time of the limiter.

In addition, the results from the Quartz MicroBalance (QMB) [18] measuring the amount of carbon deposited in the inner divertor louvre indicates clearly less erosion of carbon on the divertor with mitigated ELMs. In type-I ELMy H-mode plasmas, net deposition of carbon on the QMB with a growth rate of ~0.6 nm/s was observed. However, when the large ELMs were mitigated by an application of low n perturbation fioelds, net-erosion of carbon from the QMB (~0.25 nm/s) was observed, which is mainly due to a strong reduction of the carbon flux but still having a significant deuterium flux.

3.3. COMPENSATION OF THE DENSITY PUMP-OUT E®ECT WITH GAS PUFFING ON JET

Compensation of the density pump-out e®ect due to the application of the external $n = 1$ field has been performed with gas puffing on JET. The target plasma in this experiment is chosen from the power scan in the ITER baseline scenario described in the previous section. The gas puffing started just after the injection of NBI and ~1s before the n = 1 field was applied. The total gas puffing rate has systematically increased from discharge to discharge from 4.2, 7.8, 11.9, up to 15.4×10^{21} el/s keeping the same NBI input power of 11.2 MW.

Figure 9 shows that the central line integrated electron density as function of I_{EFCC}. Without additional gas fuelling, the electron density starts to drop at I_{EFCC} = 13kAt. The reduction of $n_e l$, $n_e l$, due to the pump-out effect does linearly depend on the amplitude of I_{EFCC}. However, a contiguous drop in $n_e l$ is observed even after I_{EFCC} reached the °at top value, which indicates that full stationarity hasn't been reached in the unfuelled case. The Greenwald fraction, f_{GW}, drops from 0.68 to 0.55. When gas puffing is applied with a total gas rate of 7.8×10^{21} el/s, the target plasma density increased (f_{GW} = 0.73) and maintains a constant value even with application of the $n = 1$ perturbation field. The further increase of the gas fuelling rate up to 15.4×10^{21} el/s yields a Greenwald density of f_{GW} = 0.95 before application of the $n = 1$ field, however, the plasma density drop with increasing I_{EFCC} appears again after the critical I_{EFCC} of 13 kAt was exceeded. These results demonstrate that there is an optimized fuelling rate for the compensation of the density pump-out effect. Nevertheless, the plasma confinement becomes worse when the plasma density is chosen too high (close to Greenwald Limit) in the low triangularity target plasma. There is a limitation to achieve a high plasma density without degradation of plasma confinement with an $n = 1$ field in low triangularity plasmas. Further investigation of the ELM control with an $n = 1$ field will be performed in high density, high triangularity plasmas in the near future. However, it should be noted that there is no further drop of the density during the flat top of *IEFCC* in the discharges with gas fuelling.

The influence of an $n = 1$ field on the profiles of n_e, T_e and p_e for the discharges with no gas fuelling and optimized gas fuelling at a rate of 7.8×10^{21} el/s. Without gas fuelling, the application

of an $n = 1$ field lets the density drop everywhere from core to edge while the electron temperature increases in the core stronger than that at the plasma edge. By application of gas fuelling, both, plasma density and temperature in the plasma core remain the same as before. However, an increase of the edge density and a drop in the edge temperature are observed. The electron density profile is getting flatter with gas fuelling, while the temperature profile becomes steeper in the plasma core. A similar influence of an $n = 1$ field on the electron pressure profile has been observed in plasmas with and without gas fuelling.

Below the optimised fuelling rate, the influence of gas fuelling on the frequency of the mitigated ELMs is weak. Once the gas rate increases over the optimised value, a clear rise of the ELM frequencies is observed in both cases with and without the $n = 1$ field.

3.4. TOROIDAL ROTATION BRAKING WITH LOW N PERTURBATION ¯ELDS

Self-similar braking of plasma toroidal rotation (v_{tor}) has been observed at plasma core during application of EFCC in both, $n = 1$ and $n = 2$ configurations while a strong braking appears at the plasma edge near the pedestal. Figure 10 (*a*) shows the time evolutions of plasma toroidal rotation v_ϕ and *IEFCC* to that measured before application of EFCC in a target plasma ($I_p = 1.4$MA, $B_t = 1.84$T; $q_{95} = 4.6$, $P_{NBI} = 10$MW). The normalized toroidal ration as a function of I_{EFCC} is shown in fig.10 (*b*). v_ϕ braking follows the increase of the EFCC coil current and depends linearly on the effective perturbation field. The edge braking effect near the plasma pedestal ($R = 3.69–3.77$m) is stronger than the braking in the plasma core ($R = 3.1–3.62$m). Here the R is the plasma major radius and the plasma magnetic axis is ~3:04m in this discharge.

Figure 11 shows the normalized toroidal rotation velocity to that measured before application of EFCC at $I_{EFCC} = 30$kAt ($n = 1$ configuration) as a function of q_{95}. In this experiment, the plasma current is changed pulse by pulse from 1.4MA to 2.0MA at constant B_t) of 1.84T. No locked mode excited with $I_{EFCC} \leq 30$ kAt even with $q_{95} = 3$. No clear dependence of toroidal braking with $n = 1$ field on q_{95} has been observed in a wide window of $q_{95} = 4.8–3.0$. There is also no clear dependence of toroidal rotation braking on the plasma collisionality has been observed in the range $\nu^* = 0.004–0.012$.

The strong braking of core MHD rotation has also been observed by Mirnov coils. When the $n = 1$ field was applied, the frequency of the sawteeth precursor mode, f_{PC}^{ST} at in the plasma core was reduced from 10 to 6kHz when the I_{EFCC} increased up to 24 kAt. There is a critical value of the I_{EFCC} observed above which the f_{PC}^{ST} started to decrease. The changes of f_{PC}^{ST} are linearly dependent on the amplitude of the I_{EFCC} after the critical value (~12kAt) of the I_{EFCC} has been exceeded. Similar plasma braking effect has been observed with $n = 1$ and $n = 2$ fields when a same EFCC coil current was applied. Since the amplitudes of $n = 2$ effective perturbations in $n = 2$ EFCC configuration is by a factor of 4 smaller than that of $n = 1$ harmonic in $n = 1$ EFCC configuration as shown in figure 1, this indicates that non-resonant magnetic braking could play a role in affecting the plasma rotation [19].

The interaction of the $n = 2$ field with the pre-seeded $m/n = 3/2$ NTM has been observed. Figure 12 shows the frequency spectrum of a Mirnov coil. The time evolution of I_{EFCC} is plotted in the same figure. The $m/n = 3/2$ NTM was triggered by a large perturbation of sawtooth crash before the EFCC is applied. There is no increasing of the amplitude of the 3/2 mode even I_{EFCC} is increased up to 32kAt. The frequency of the 3/2 mode reduced from 17kHz to 10kHz, while f_{PC}^{ST} is reduced with a similar factor from 8kHz to 5kHz. There is no clear difference of the rotation braking effect by the $n = 2$ fields for the plasmas with and without a 3/2 NTM. This result indicates the $m/n = 3/2$ sideband of the EFCC induced field does not penetrate deeply into the plasma core where the screening effects due to plasma rotation can not be neglected.

3.5. ELM CONTROL IN A LOW ROTATION PLASMA WITH TF RIPPLE

JET is equipped with a set of 32 Toroidal Field (TF) coils with two independent power supplies for the odd and the even set of coils. The minimal toroidal field ripple with an equal current in TF coils is $\delta B_T \sim 0.08\%$ at the nominal separatrix radius in the outer midplane. By selecting the appropriate differential current between the odd and even set of coils, the TF ripple can be adjusted in a controlled way. Both, the density pump-out and the momentum braking have been also observed in the plasmas with an increased TF ripple [20]. However, the mechanisms of plasma braking are different: drag due to resonant and non-resonant magnetic braking vs counter torque due to ion losses.

ELM control with $n = 1$ field has been applied for a low rotation plasma with TF ripple up to 0.8%. The target type-I H-mode plasma ($I_p = 2.0$MA, $B_t = 2.2$T; $q_{95} = 3.6$) is maintained by NBI with $P_{NBI} = 10.8$MW. With application of $n = 1$ field with $I_{EFCC} = 32$kAt, an increasing of the ELM frequency has been observed in these plasmas with TF ripple. In the plasmas with TF ripple of 0.5% and 0.8%, the ELM becomes compound because of a less absorbed heating power with increasing of fast ion losses. However, this compound ELM becomes more regular small type-I ELM when the $n = 1$ field was applied.

Figure 13 shows toroidal plasma core rotation measured at $R = 3.04$ m as a function of TF ripple. With an increasing of TF ripple only, the plasma core rotation reduced in co-current direction and it is dropped by a factor of 3 when the TF ripple increased up to 0.8%. When the $n = 1$ field was applied, the plasma core rotation reduced by a factor of 3 in the plasma with a small ripple below 0.3% while no clear change of plasma rotation was observed with TF ripple above 0.8%.

Figure 14 shows the density Greenwald fraction as a function of TF ripple for the cases with and without $n = 1$ field. Plasma density Greenwald fraction number, n_{GW}, reduced from 0.8 to 0.62 with increasing of TF ripple up to 0.8%. With application of $n = 1$ field, the density drops by 20% in plasma with a TF ripple of 0.08%. Less density pump-out due to an application of magnetic perturbation has been observed in the plasmas with large TF ripple of 0.8%.

DISCUSSION AND CONCLUSION

The $n = 1$ fields has been also applied for mitigating the first ELMs after L-H transition. The

preliminary results show no clear influence on the first ELMs even with the same amplitude of EFCC coil current for the control of ELMs in the stationary phase.

No clear change of the locked mode threshold even in a low rotation plasma with TF ripple has been observed. This is considered due to the plasma rotation always braking down by the large amount of low n perturbation fields before the locked mode triggered.

In conclusions, the results of ELM control with the low n (n = 1, 2) perturbation fields on JET demonstrate that the frequency of ELM can be increased by a factor of 4, only limited by the available EFCC coil current. During the application of the n = 1, 2 fields, a reduction in the ELM size (ΔW_{ELM}) and ELM peak heat fluxes on the divertor target by roughly the same factor as the increase of the ELM frequency has been observed. The reduction in heat flux is mainly due to the drop of particle flux rather than the change of the electron temperature. Compensation of the density pump-out effect has been achieved by means of gas fuelling in low triangularity plasmas. An optimised fuelling rate to compensate the density pump-out effect has been identified. Similar plasma braking effect has been observed with n = 1 and n = 2 external fields when a same EFCC coil current was applied. Less toroidal rotation braking and density pump- out due to an application of magnetic perturbation has been observed in the plasmas with large TF ripple of 0.8%. Active ELM control by externally applied perturbation fields offers an attractive method for next-generation tokamaks, e.g. ITER.

ACKNOWLEDGEMENT

This work, supported by the European Communities under the contract of Association between EURATOM and FZJ, was carried out within the framework of the European Fusion Development Agreement. The views and opinions expressed herein do not necessarily reflect those of the European Commission.

REFERENCES

[1]. ITER Physics Basis, 1999, Nuclear Fusion **39** 2137
[2]. Wagner F, *et al* , 1982 Physical Review Letters **49** 1408
[3]. Connor J.W, 1998 Plasma Phys. Control. Fusion **40** 531
[4]. Loarte A, *et al* , 2003 Journal Nuclear Materials **313-316** 962
[5]. Evans T, *et al* , 2004 Physical Review Letters **92** 235003
[6]. Evans T, *et al* , 2006 Nature Phys. **2** 419
[7]. Liang Y, *et al* , 2007 Physical Review Letters **98** 265004
[8]. Liang Y, *et al* , 2007 Plasma Physics and Controled Fusion **49** B581
[9]. Liang Y, *et al* , 2008 Journal Nuclear Materials at press
[10]. Barlow I, *et al* , 2001 Fusion Eng. Des. **58-59** 189
[11]. Koslowski H.R, *et al* , 2007 Proc. 34th EPS Conf. on Plasma Physics (Warsaw, Poland) P5.135
[12]. Buttery R.J, *et al* , 1999 Nucl. Fusion **39** 1827

[13]. Schmitz O. *et al* , 2008 Proc. 35th EPS Conference on Plasma Physics
[14]. Alfier A. *et al* , 2008 Nuclear Fusion **48** 115006
[15]. Vallet J.C, *et al* , 1991 Physical Review Letters **67** 2662
[16]. Saarelma S, *et al* ,, 2008 submitted to Plasma Phys. Control. Fusion
[17]. Jachmich S, *et al* , 2007 Proc. 34th EPS Conf. on Plasma Physics (Warsaw, Poland) P5.099
[18]. Esser H.G, et al 2005 J. Nucl. Mater. **337-339** 84
[19]. Shaing K.C, 2003 Phys. Plasmas **10**, 1443
[20]. Saibene G, *et al* , IAEA-CN-165/EX/2-1, 22nd IAEA Fusion Energy Conference Geneva, Switzerland, 13 - 18 October 2008

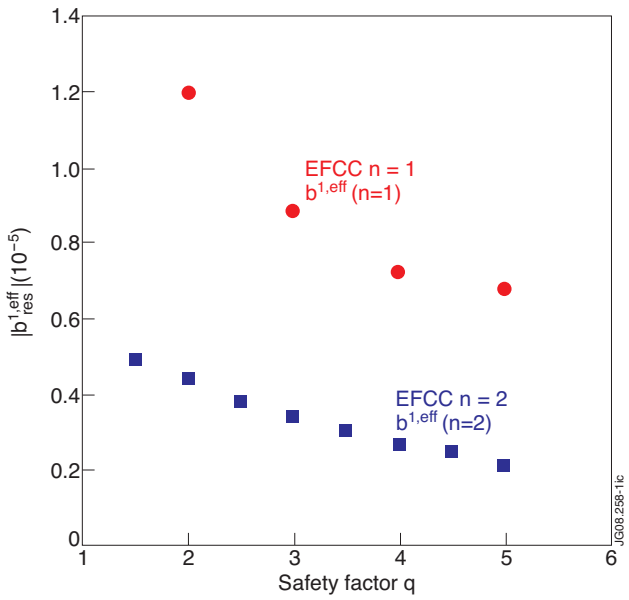

Figure 1: Effective resonant magnetic perturbation for 1kAt in the EFCCs in n = 1and n = 2 configurations.

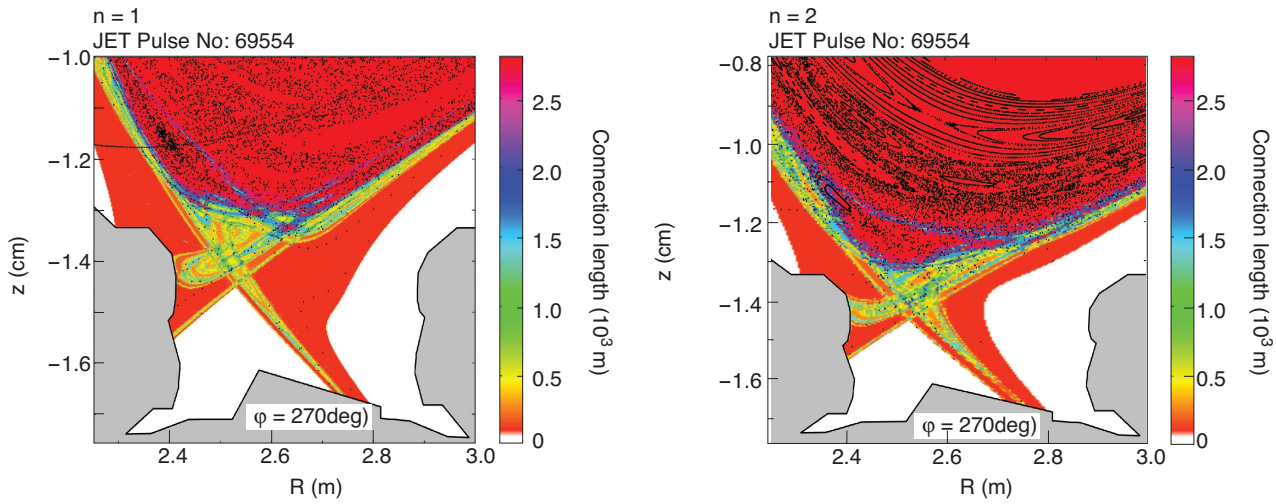

Figure 2: Poincar and laminar plot for (upper) n = 1 and (lower) n = 2 EFCC configuration with I_{EFCC} = 32 kAt.

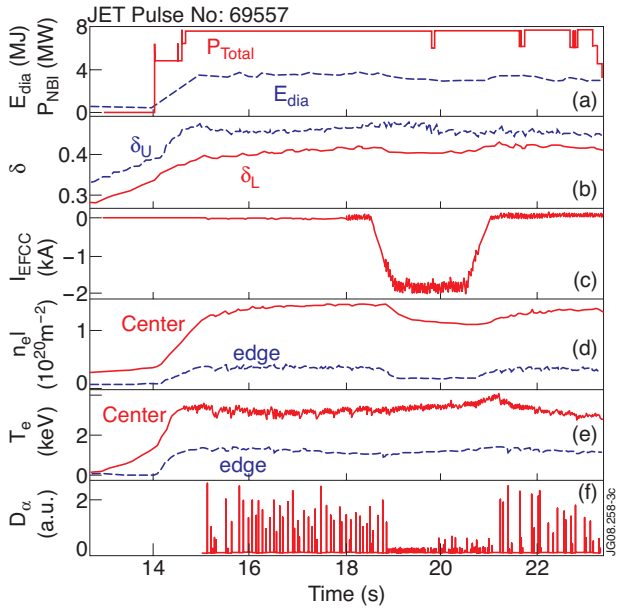

Figure 3: (a)-(f) Overview on a typical ELM control experiment in a high triangularity plasma.

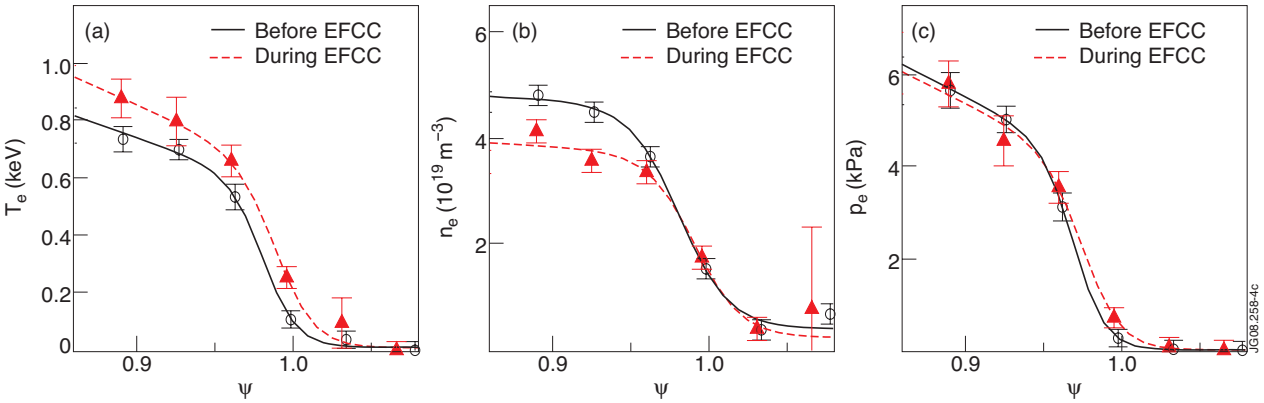

Figure 4: The radial profiles in normalized flux coordinate (Ψ) before (full line and empty circles) and during (dashed line and full triangle) control.

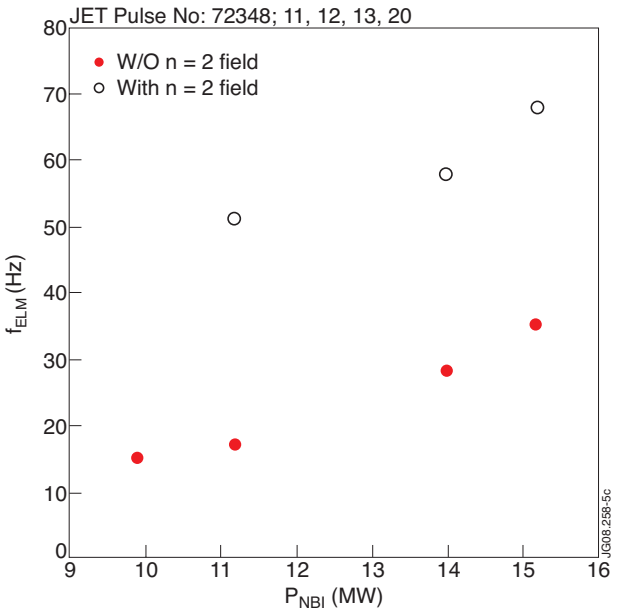

Figure 5: Heating power dependence of ELM frequency measured during the phases with and without an n = 1 field.

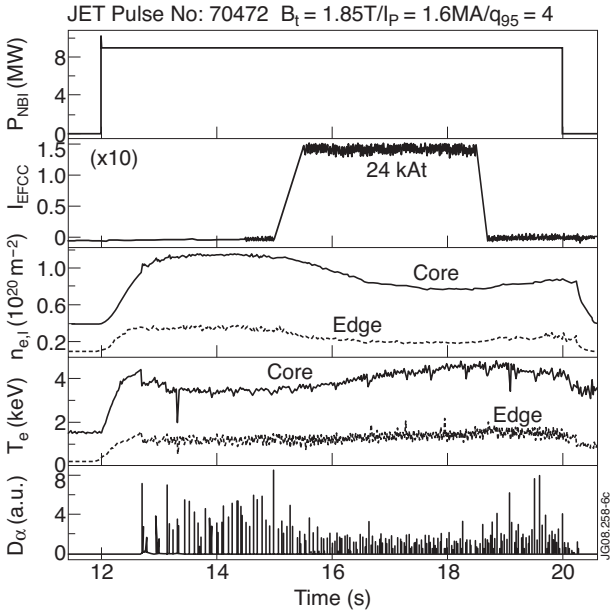

Figure 6: Overview on a typical ELM control experiment in a low trangularity plasma on JET.

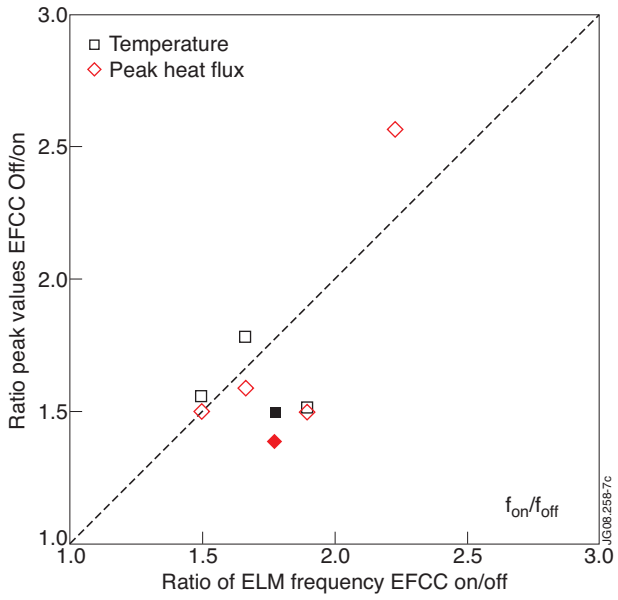

Figure 7: Heat load control efficiency with an n = 2 field.

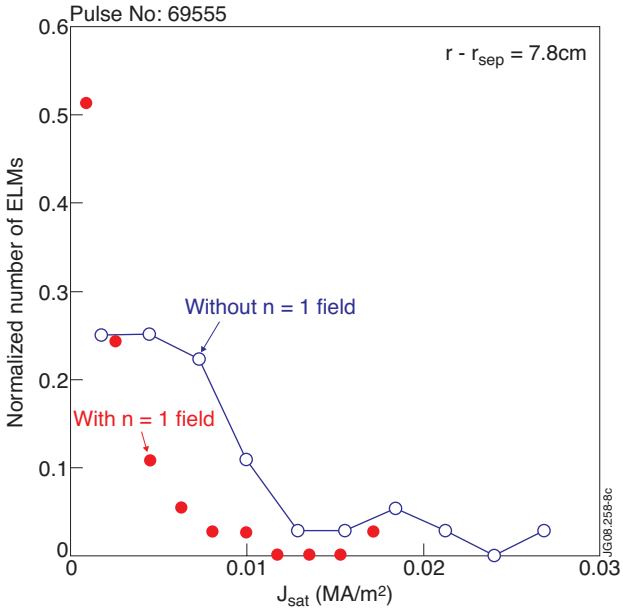

Figure 8: Normalized number of ELMs as a function of the saturation current measured during ELMs with and without an n = 1 field.

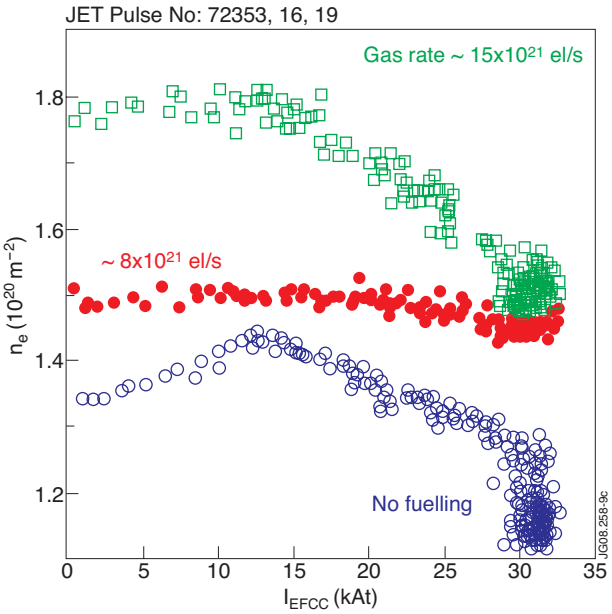

Figure 9: Central line-integrated density as a function of I_{EFCC} for the discharges with and without gas fuelling.

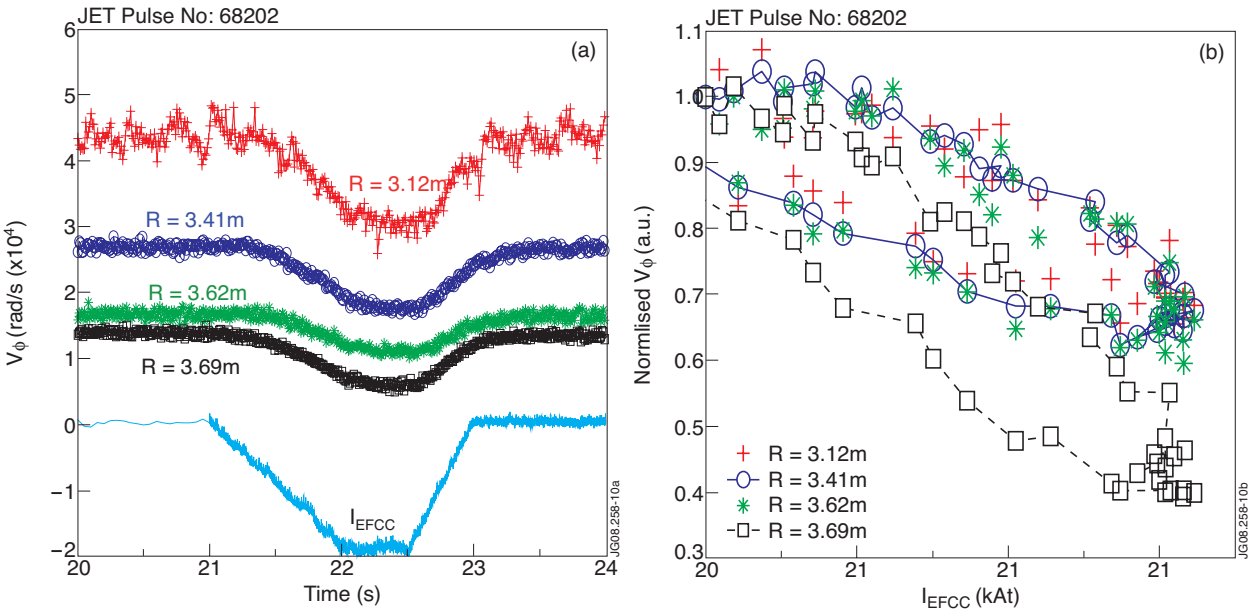

Figure 10: (a) Time evolution of plasma toroidal angle velocity at different radii and I_{EFCC}. (b) Normalized angular frequency to that before EFCC switched on as a function of I_{EFCC}.

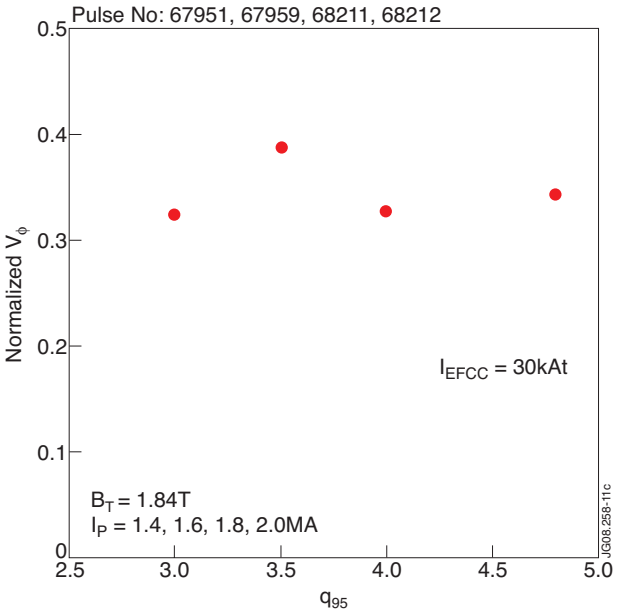

Figure 11: q_{95} dependance of normalized angular frequency to that before EFCC switched on.

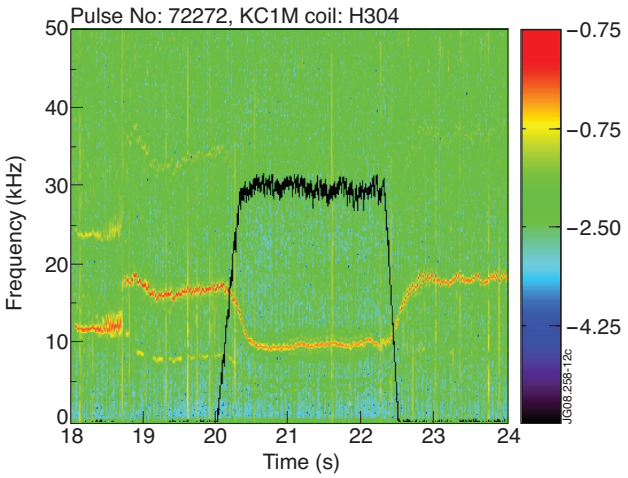

Figure 12: Frequency spectrum of a pick-up coil measurement (I_p = 1.4MA, B_t = 1.85T; P_{NBI} = 11MW; I_{EFCC} = 32kAt).

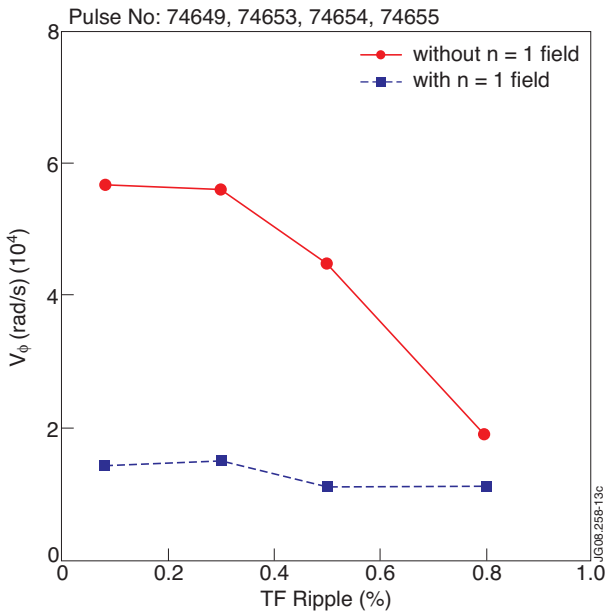

Figure 13: Plasma toroidal rotation at R = 3.04m as a function of TF ripple for the cases with and without n = 1 field.

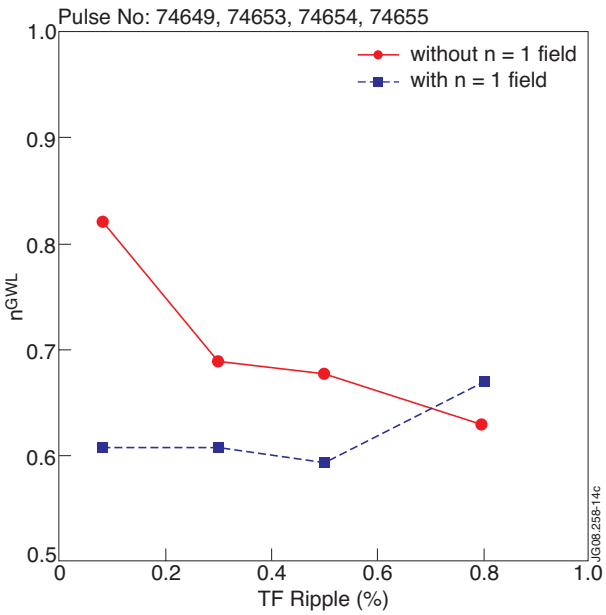

Figure 14: Greenwald fraction as a function of TF ripple for the cases with and without n = 1 field.